

Liquid Crystal Ordering and Isotropic Gelation in Solutions of Four-Base-Long DNA Oligomers

Tommaso P. Fraccia,^{†,||} Gregory P. Smith,[‡] Lucas Bethge,[§] Giuliano Zanchetta,[†] Giovanni Nava,[†] Sven Klussmann,[§] Noel A. Clark,[‡] and Tommaso Bellini^{*†}

[†]Dipartimento di Biotecnologie Mediche e Medicina Traslazionale, Università di Milano, via Fratelli Cervi 93, I-20090 Segrate (Milan), Italy

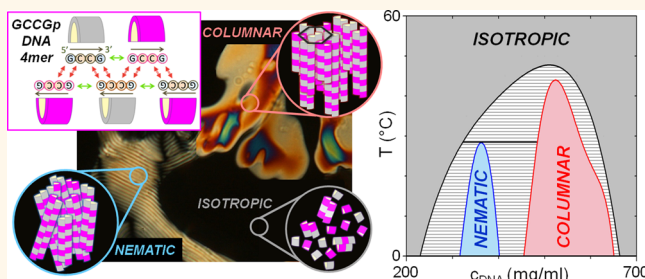
[‡]Department of Physics and Liquid Crystal Materials Research Center, University of Colorado, Boulder, Colorado 80309-0390, United States

[§]NOXXON Pharma AG, Max-Dohrn-Strasse 8-10, 10589 Berlin, Germany

^{||}Dipartimento di Scienze Umane e Promozione della Qualità della Vita, Università San Raffaele di Roma, via di Val Cannuta, 247, I-00166 Rome, Italy

Supporting Information

ABSTRACT: Liquid crystal ordering is reported in aqueous solutions of the oligomer 5'-ATTAp-3' and of the oligomer 5'-GCCGp-3'. In both systems, we quantitatively interpret ordering as stemming from the chaining of molecules *via* a "running-bond" type of pairing, a self-assembly process distinct from the duplex aggregation previously reported for longer oligonucleotides. While concentrated solutions of 5'-ATTAp-3' show only a columnar liquid crystal phase, solutions of 5'-GCCGp-3' display a rich phase diagram, featuring a chiral nematic phase analogous to those observed in solutions of longer oligonucleotides and two unconventional phases, a columnar crystal and, at high concentration, an isotropic amorphous gel. The appearance of these phases, which can be interpreted on the basis of features of 5'-GCCGp-3' molecular structure, suggests distinctive assembly motifs specific to ultrashort oligonucleotides.



KEYWORDS: liquid crystals, self-assembly, DNA nanotechnology, origin of life, coaxial stacking of DNA

The motifs of supramolecular ordering of oligonucleotides constitute a field of investigation constantly enriched with new findings, including sequence-directed self-assembly,¹ formation of low-concentration hydrogels,^{2,3} base-stacking driven structures,^{4,5} and various forms of liquid crystalline (LC) long-range ordering and of phase separations.^{6–9} Here, we report that solutions of ultrashort DNA oligomers have a (surprisingly) rich phase diagram at and above room temperature (T) and at concentrations about 1 M nucleobases, featuring chiral nematic and columnar LC phases, columnar crystals, and high-density isotropic gel.

Previous investigations described a mechanism for LC ordering of DNA oligomers through a three-step self-assembly process.⁶ First, oligomers hybridize into duplexes, which are stable at T below their melting. Second, duplexes form linear aggregates. Such aggregation is mediated by either base stacking of terminal bases in the case of blunt-ended duplexes or by pairing of terminal sections when duplexes terminate with interacting overhangs. Third, linear aggregates align and form a LC phase. Although these steps mutually strengthen, with LC ordering enhancing chaining and duplex stability, no LC

ordering was previously observed for oligomers too short to form stable duplexes. Indeed, when we observed that LC phases of six-base-long oligomers were pushed at large DNA concentration (c_{DNA}) and low T ,⁶ we assumed that four-base-long oligomers would not order, being that their duplexes are unstable at all T above freezing at "ordinary" (less than micromolar) concentrations. Moreover, shorter oligomers imply more flexibility of the aggregates, which is a destabilizing factor for LC ordering.¹⁰

Our previous results on the collective ordering of DNA and RNA oligomers led us to speculate on a possible role of such supramolecular structuring in the first appearance of nucleic acid polymers in the early Earth. Indeed, current "RNA world" scenarios envision a self-sustaining condition formed by a pool of polymers with simultaneous catalytic and information-carrying capacity.¹¹ However, the availability of long enough

Received: June 1, 2016

Accepted: August 29, 2016

Published: August 29, 2016

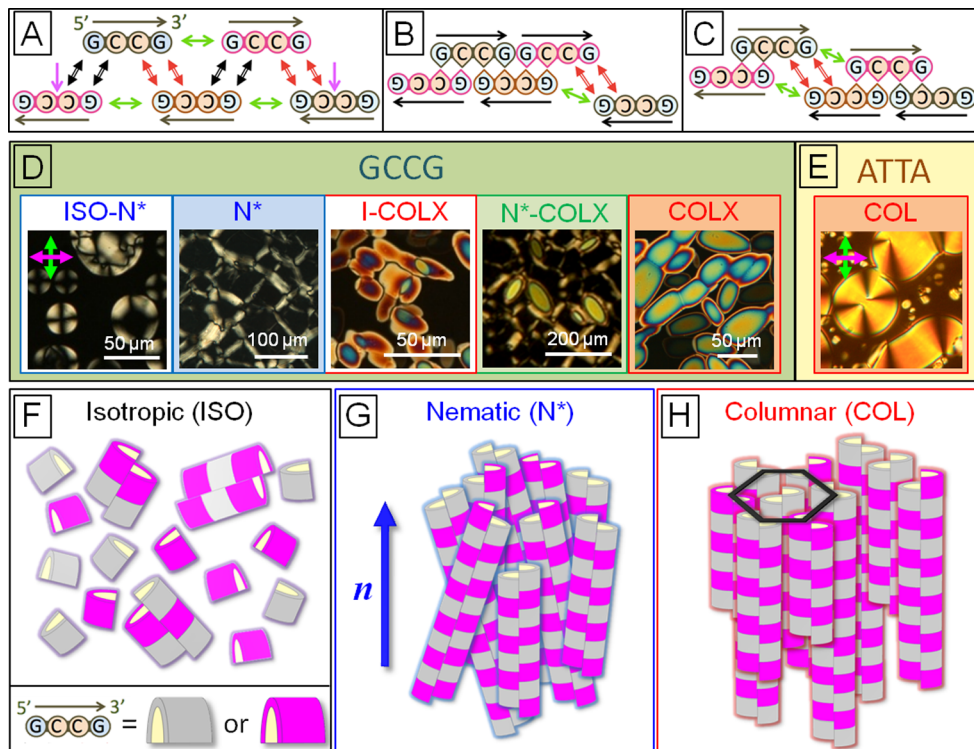


Figure 1. Modes of assembly of the 4mers 5'-GCCGp-3' and 5'-ATTAp-3'. (A) Pairing and stacking interactions at play in the stability of the GCCG aggregates: Watson–Crick GC/CG quartets (black arrows) and CG/GC quartets (red arrows), coaxial stacking (green arrows), dangling end stacking (between the bases as marked by pink arrows). (B, C) Interactions at play between an aggregate and a monomer (B) and between two aggregates (C). (D, E) Pictures by polarized transmission optical microscopy of thin cells of GCCG (D) and ATTA (E) at $T = 10\text{ }^{\circ}\text{C}$ and distinct concentrations (from left to right $c_{\text{DNA}} = 650\text{ mg/mL}$, $c_{\text{DNA}} = 260\text{ mg/mL}$, $c_{\text{DNA}} = 365\text{ mg/mL}$, $c_{\text{DNA}} = 450\text{ mg/mL}$, $c_{\text{DNA}} = 500\text{ mg/mL}$ and $T = 25\text{ }^{\circ}\text{C}$, $c_{\text{DNA}} = 570\text{ mg/mL}$). (F–H) Sketches of the self-assembly of DNA 4mers, represented by semicylinders with alternate gray and violet colors to appreciate their binding, in the different phases: isotropic phase formed by single strands and short chains (F), chiral nematic (N^*) LC phase in which longer chains are orientationally ordered (G), and columnar (COL) LC phase in which parallel columns free to slide past each other form an hexagonal 2D lattice (H). Structure of COLX phase is described in Figure 3.

nucleic acid chains, sufficiently homogeneous in the main chain and carrying a small set of weakly polymorphic side groups capable of pairing, is yet to be understood. We recently showed that the LC ordering of 12-base-long DNA oligomers efficiently acts as a template that strongly promotes their abiotic chemical ligation into long chains, involving in this process only those oligomers capable of pairing and chaining.^{8,12,13} Here, we show that DNA 4mers are also able to develop LC ordering, thus strengthening our proposed prebiotic scenario by reducing the molecular size that could self-catalyze their own lengthening.

The molecules we investigated and report about in this paper are 5'-GCCGp-3' and 5'-ATTAp-3' (GCCG and ATTA, preparation and purification details in the *Methods*), partially self-complementary and with interacting overhangs. Their Watson–Crick “running-bond” chaining mode of GCCG is sketched in Figure 1A, while the one of ATTA is strictly analogous. Quite clearly, in this case there is no distinction between duplex formation and linear aggregation. Rather, hybridization and chaining necessarily take place in a single continuous process in which the bonding of each GCCG or ATTA molecule to an existing chain (Figure 1B) and the merging of different chains (Figure 1C) are characterized by a free energy gain. This condition leads to equilibrium states characterized by a distribution of lengths, ranging from single dissociated oligomers to multimolecular aggregates. As is typical for “living polymers”,¹⁴ such distribution is expected to be

exponential, with characteristic length depending on interaction strength and T , as discussed below.

RESULTS

Pairing Modes of ATTA and GCCG and Their Thermal Stability. In Figure 1A–C we sketch the various interactions that contribute to the formation of the linear aggregates. Indeed, besides the contributions to the free energy from the formation of quadruplets, *i.e.*, pairs of adjacent Watson–Crick bonds between distinct strands whose free energy is typically determined in the frame of nearest neighbor (NN) model¹⁵ (double black and red arrows in Figure 1A), important additional contributions come through “coaxial stacking”, *i.e.*, the stacking interactions of chemically disconnected but physically contacting paired bases (green arrows in Figure 1A), and through “dangling ends”, *i.e.*, the stacking of an unpaired single base adjacent to a C–G or A–T pair (in the position marked by a pink arrow in Figure 1A). Coaxial stacking and dangling end are essential here and make the binding of the chains much stronger than that in the formation of lone pairs of GCCG and ATTA. It should also be noticed that, because of its low molecular weight, the molar concentration of GCCG and ATTA where LC phases are found is in the range 0.2–0.6 M. At these large concentrations, molecular associations with a binding coefficient as low as a few $k_{\text{B}}T$, such as those here considered, become relevant.

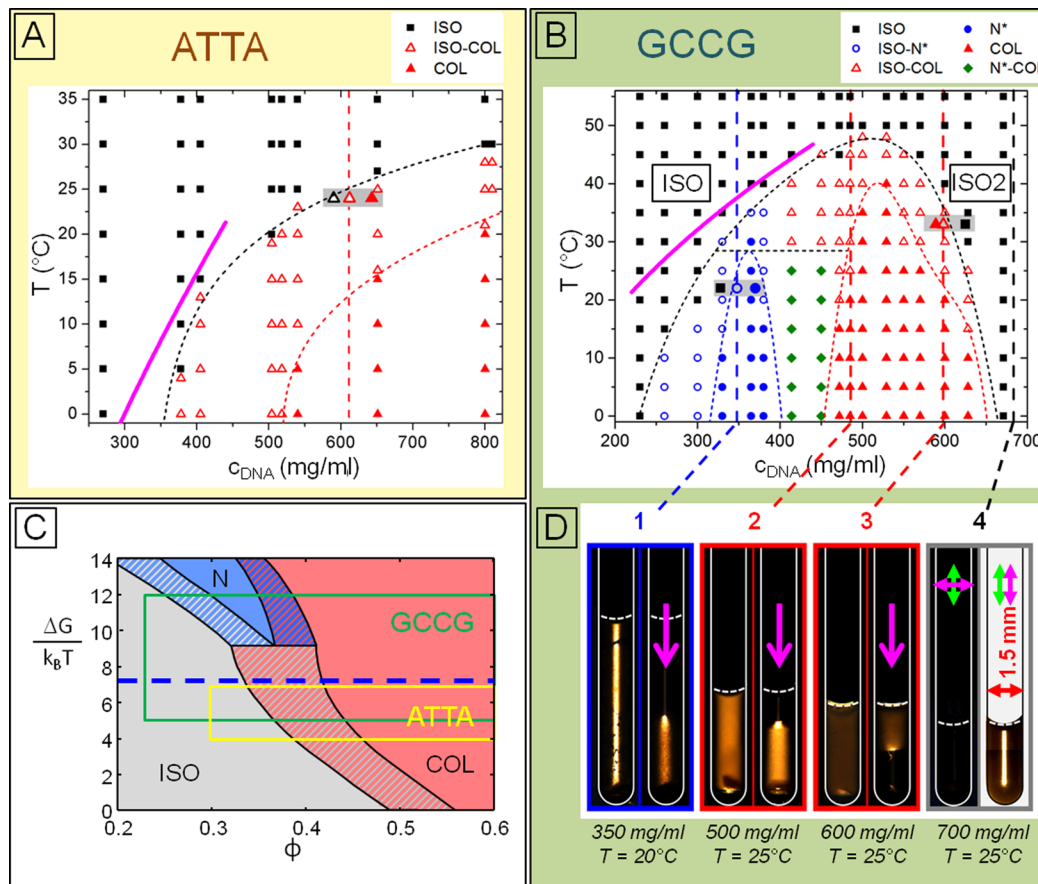


Figure 2. Phase diagram of 5'-GCCGp-3' and 5'-ATTAp-3'. (A, B) c_{DNA} -T phase diagrams for ATTA (A) and for GCCG (B). Symbols indicate: ISO and ISO2 phase (solid black squares), ISO-N* coexistence (empty blue circles), N* phase (solid blue circles), ISO-COL and ISO-COLX coexistence (empty red triangles), N*-COLX coexistence (solid green diamond), COL and COLX phase (solid red triangles). Thin dashed lines guide the eyes to identify the phase boundaries (black, ISO; blue, N*; and red, COL/COLX). Magenta lines mark the ISO side of the ISO-LC phase coexistence according to the model of ref 19 implemented with ΔG_{ATTA} and ΔG_{GCCG} obtained from melting temperature measurements. Vertical lines and 1–4 labels mark the c_{DNA} where capillaries were prepared and investigated. Symbols over a gray shading indicate the c_{DNA} of the two coexisting phases measured after cutting centrifuged capillaries at the meniscus. (C) $\Phi - \Delta G/k_B T$ phase diagram for DNA duplexes with L/D = 0.5 from ref 18; solid contours highlight the volume fraction–energy regions investigated in the experimental phase diagrams of ATTA (yellow) and GCCG (green); blue dashed line indicate the experimental $\Delta G_{\text{MIN}}/k_B T \approx 7.3$ for the nematic ordering. (D) Pictures of the larger capillary positioned between crossed polarizers before and after centrifugation (magenta arrow) showing ISO-N* (1), ISO-COLX (2), COLX-ISO2 (3), and ISO2 (4) at c_{DNA} and T as indicated.

A straightforward approach to estimate the strength of ATTA and GCCG base-paired chains is to measure their thermal melting through the fluorescent emission $I_F(T)$ of ethidium bromide (EtBr), a fluorophore whose fluorescence quantum yield markedly increases upon its intercalation between paired bases of DNA. We find that, in both systems, EtBr fluorescence decay reveals a single, broad thermal transition occurring at a T depending on c_{DNA} , which at the highest concentrations reaches 60 °C, a remarkably large value. While normally EtBr melting curves are interpreted in terms of duplex melting, here this notion should be revisited because of the ATTA- and GCCG-chaining mode that leads to a distribution of aggregate lengths. In this case, instead, the fraction of bonded bases revealed by I_F provides information on the mean chain length. Toward this end, we adopted the description of linear aggregation provided by recent models that enable calculating the chain length distribution cylinders having adhesive bases with interaction strength ΔG .^{13,14} We thus model our chains as cylinders whose size is that of two-base-long duplexes, since this corresponds to the lengthening of the aggregates for each addition of a 4mer. Within this assumption, we analyzed our $I_F(T)$ data and

determined the free energy gain ΔG that favors the chaining of ATTA (ΔG_{ATTA}) and GCCG (ΔG_{GCCG}). Since these values are determined from conditions in which the monomeric ATTA and GCCG are a small fraction of the population (making the process in Figure 1B of minor importance), we argue that the values of $\Delta G_{\text{ATTA}}(T)$ and $\Delta G_{\text{GCCG}}(T)$ that we extract represent the interchain bonding free energy shown in Figure 1C. $I_F(T)$ data and analysis are reported and extensively discussed in the Supporting Information.

The values obtained for $\Delta G_{\text{ATTA}}(T)$ and $\Delta G_{\text{GCCG}}(T)$ (in Table S1) can be compared with those calculated with the well-established NN thermodynamic parameters for DNA stability to obtain further information on coaxial stacking. Indeed, while the thermodynamic stability of quadruplets and the contribution of dangling ends is rather well determined, the value of coaxial stacking has been studied less and with quite different outcomes.^{16,17} Therefore, by subtracting from $\Delta G_{\text{ATTA}}(T)$ and $\Delta G_{\text{GCCG}}(T)$ the effects of quadruplets and dangling ends, we obtained a determination of the thermodynamic parameters of coaxial stacking. Namely, for nicks A-A/TT we find $\Delta H_{\text{coax}}^{\text{AA}} = -3.7$ kcal/mol and $\Delta S_{\text{coax}}^{\text{AA}} = -4.8$ cal/(mol K), while for nicks

G–G/CC we find $\Delta H_{\text{coax}}^{\text{GG}} = -12.6 \text{ kcal/mol}$ and $\Delta S_{\text{coax}}^{\text{AA}} = -32.7 \text{ cal}/(\text{mol K})$. These values, which are in this case referred to a condition of increasing ionic strength due to phosphate dissociation, are included in the wide interval between the results of two studies reported in literature^{16,17} (see the SI).

Phase Behavior of ATTA and GCCG. We have studied the phase behavior of solutions of GCCG and ATTA without added salt at concentrations $c_{\text{DNA}} > 200 \text{ mg/mL}$ and up to $c_{\text{DNA}} \approx 800 \text{ mg/mL}$, above which samples are difficult to handle and homogeneity is hard to obtain. This range of concentration, corresponding to 1–2.5 M phosphate groups, ensures the presence of a large concentration of Na^+ -dissociated counterions and therefore essentially complete screening, a condition that has been taken into account in the quantitative discussion of the results. Exploration by polarized transmission optical microscopy (PTOM) of the phase behavior of solutions in thin flat cells (examples in Figure 1D,E) enabled identification of domains in the $c_{\text{DNA}}-T$ plane exhibiting birefringent textures typical of liquid crystal ordering as well as domains in which we found coexistence of birefringent and isotropic phases. The 4mers self-assembly in the isotropic and LC phases are sketched in Figure 1F–H.

The PTOM textures observed in ATTA cells indicate that this system can order into a columnar (COL) LC phase (Figure 1E) in the $c_{\text{DNA}}-T$ range reported in Figure 2A. The PTOM textures of GCCG indicate a richer phase behavior, featuring chiral nematic (N^*) LC ordering and the formation of a more rigid ordering that we identify as a columnar crystal phase (COLX), Figure 1D. The domains for the N^* and COLX phases are reported in Figure 2B. In both ATTA and GCCG phase diagrams, black, blue, and red symbols indicate the isotropic I, N^* , and COL/COLX phase, respectively. Open symbols indicate N^* -ISO and COL/COLX-ISO coexistence. Green dots mark N^* -COLX coexistence. In both phase diagrams, LC ordering, although in coexistence with the isotropic phase, is remarkably stable, found at higher temperatures and lower concentrations than in longer blunt-ended oligomers (6–10mers). The phase behavior of GCCG shows a few remarkable features not found previously in other DNA oligomers nor in the ATTA phase diagram: (i) the appearance of an isotropic phase which replaces LC ordering at high c_{DNA} ; (ii) a resulting bell-shaped structure of the LC region in the phase diagram; and (iii) a crystalline columnar phase, COLX, replacing the COL LC phase found in other DNA oligomers and in ATTA solutions. These topics are analyzed and discussed in the following sections.

Quantitative Analysis of the Phase Diagrams. Having determined the association free energies $\Delta G_{\text{ATT}}^{\text{AA}}$ and $\Delta G_{\text{GCCG}}^{\text{AA}}$ involved in the molecular assembly puts us in a position to quantitatively compare the phase diagrams in parts A and B of Figure 2 with the prediction of theoretical models for the collective behavior of cylindrical monomers undergoing base-to-base aggregation.^{18,19}

First, there is a qualitative difference between the phase diagram of ATTA, in which the N^* phase is absent, and that of GCCG, where instead it is found. According to ref 18, the nematic phase requires stronger bonds than the COL phase. This is shown in Figure 2C, where we report the phase diagram computed in ref 18 for cylinders with an axial ratio 0.5, the closest to our conditions among the values considered in that paper. As shown, the range in which the nematic phase is stable is small and bonded in energy. This is a consequence of the fact that the N^* ordering can be found only at concentrations lower

than those of the COL phase, where at higher T , the mean aggregation length is not enough to induce LC ordering. Specifically, Figure 2C indicates that the N^* phase requires end-to-end interactions to be larger than a value ΔG_{MIN} that, for an axial ratio of 0.5, is predicted to be $\Delta G_{\text{MIN}}/k_{\text{B}}T \approx 9$. Correspondingly, the concentration of maximum stability for the nematic phase is expected to be at a cylinder volume fraction of about 0.37, roughly equivalent to $c_{\text{DNA}} = 380 \text{ mg/mL}$ (see the SI.). Remarkably, our observed phase diagrams nicely agree with this prediction. At $T = 30 \text{ }^{\circ}\text{C}$, the largest T at which the N^* phase is found, $\Delta G_{\text{GCCG}} \approx 7.3 k_{\text{B}}T$, which can be assumed to be the ΔG_{MIN} for our experimental system (blue dashed line in Figure 2C), and $c_{\text{DNA}} \approx 370 \text{ mg/mL}$. Instead, even at $T = 0 \text{ }^{\circ}\text{C}$, the lowest T here explored, $\Delta G_{\text{ATT}} \approx 7 k_{\text{B}}T$, insufficient for the appearance of nematic ordering. The intervals of energies and volume fraction of equivalent cylinders explored in the experimental phase diagram are $5 k_{\text{B}}T < \Delta G_{\text{GCCG}} < 12 k_{\text{B}}T$ and $\Phi > 0.23$ for GCCG and $4.4 k_{\text{B}}T < \Delta G_{\text{ATT}} < 7 k_{\text{B}}T$ and $\Phi > 0.3$ for ATTA, highlighted by green and yellow contours in Figure 2C, respectively.

Furthermore, the same model of ref 19 that we used to extract the free energies enables calculation of the region of the phase diagram where LC ordering is expected. Specifically, the model enables determining the ISO side of the ISO–N phase coexistence (which can be extended to ISO–LC since the model does not include a distinction between N and COL phases). We thus performed this calculation using ΔG_{GCCG} and ΔG_{ATT} . The results are plotted in parts A and B of Figure 2 as purple lines in the concentration interval of confidence for the model (200–400 mg/mL, further discussion in the SI). The agreement is excellent in both cases.

The phase diagram of GCCG in Figure 2B differs from that in Figure 2C by the presence, at large concentrations, of an isotropic phase which appears to be a specific feature of this system, since upon dehydration DNA LC phases quite generally transform into more ordered, typically crystalline, states. In the case of GCCG, however, upon increasing c_{DNA} the COLX phase transforms into an isotropic state, here indicated as ISO2. This was repeatedly tested in evaporative cells at constant T , in which as c_{DNA} grows, the system horizontally crosses the phase diagram to eventually enter the ISO2 state, which is maintained up to complete dehydration (see the SI). This was also tested by preparing a sample in a 1.5 mm diameter glass capillary by inserting 5.6 mg of lyophilized GCCG at its bottom and serially adding water to span c_{DNA} through the whole range of interest. At each concentration, the samples were equilibrated, observed at different T , and gently centrifuged at given T s. Pictures of the capillaries before and after centrifugation are reported in Figure 2D for the values of c_{DNA} marked in Figure 2B by vertical lines and labels 1–4. Once separated by centrifugation, the coexisting phases remained indefinitely stable in the tubes at the sedimentation temperature, indicating an equilibrium state. We confirmed that in coexistence densities are ordered as $c_{\text{DNA}}(\text{ISO}) < c_{\text{DNA}}(\text{N}^*) < c_{\text{DNA}}(\text{COLX}) < c_{\text{DNA}}(\text{ISO2})$. By centrifuging capillary 1 (350 mg/mL) at 20 °C, the N^* phase sediments at the bottom, while the ISO phase floats on top. A similar result is found in capillary 2 ($c_{\text{DNA}} = 500 \text{ mg/mL}$) at 35 °C for the COLX phase. The behavior is reversed in capillary 3 ($c_{\text{DNA}} = 600 \text{ mg/mL}$) at 35 °C in which centrifuging leads to the sinking of the ISO2 phase and floating of COLX. Capillary 4 remains featureless under centrifugation, compatible with a homogeneous ISO2 phase.

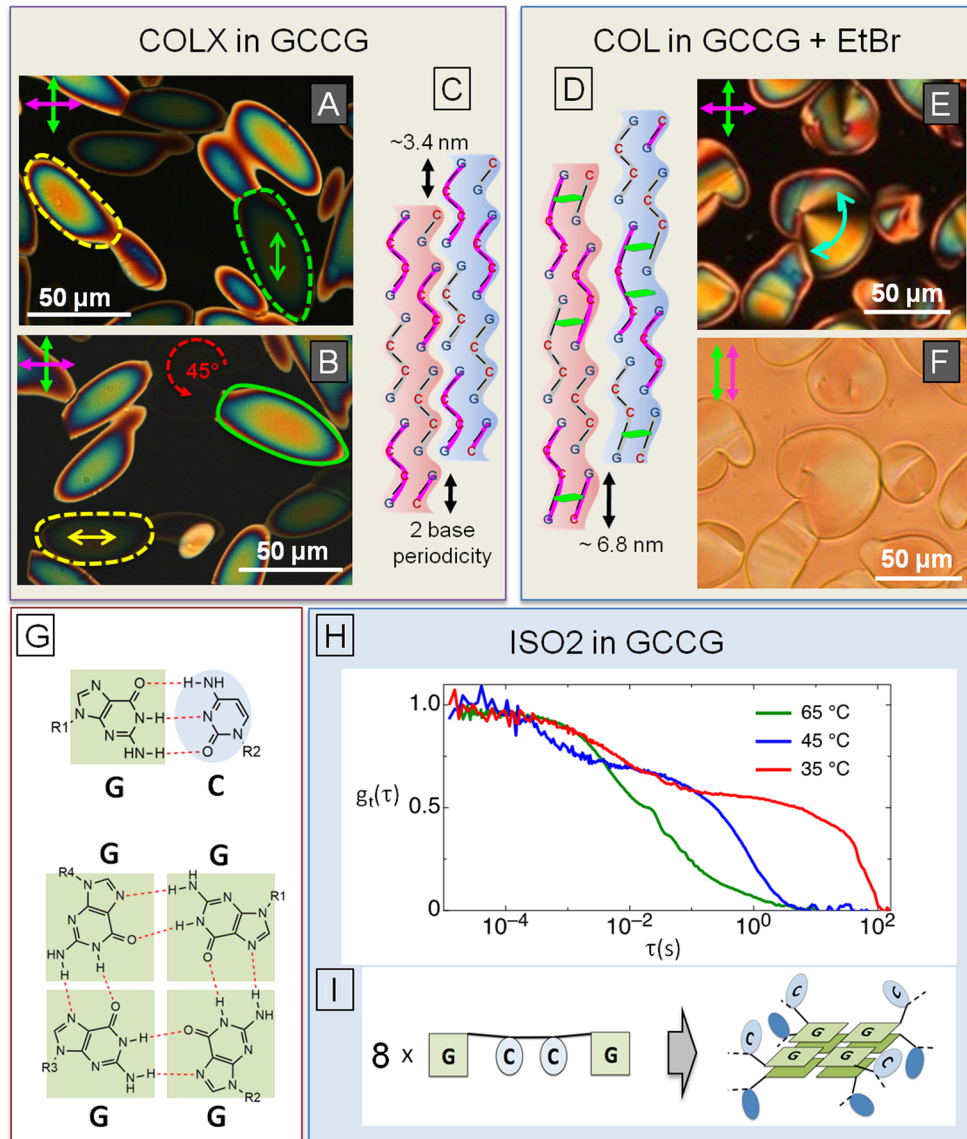


Figure 3. Description of the liquid crystalline phases of GCCG. (A, B) Polarized optical microscopy pictures between crossed polarizers of the same portion of a thin cell with COLX domains. Domains marked with a yellow and green dashed line contour show extinction and maximum brightness upon rotating the cell 45°. Yellow and green arrows indicate the optical axis (axis of least refractive index), uniform within each domain. (C) Sketch of two GCCG aggregates showing the two-base-long periodicity, which enables longitudinal locking. The shape modulation in the drawing is intended to indicate a steric modulation or a modulation of flexibility or of interaction strength between the bases of distinct aggregates. (D) Periodicity and locking mechanism disrupted by the random intercalation of EtBr (green segments). (E) Polarized optical microscopy pictures of a domain of GCCG + EtBr showing fan-shaped textures typical of COL LC ordering (light blue arrow indicates the distorted optical axis). (F) Transmission microscopy picture between parallel polarizers showing that the absorbance from EtBr is modulated following the direction of the optical axis, confirming intercalation and thus orientational order. (G) Guanine (green shading) and cytosine (blue shading) form Watson–Crick bond (left-hand side) and quadruplex bond (right-hand side). (H) Time-averaged intensity correlations of the scattered light ($\lambda = 532$, angle $\approx 90^\circ$) from a thin capillary in ISO2 phase ($c_{\text{DNA}} = 700 \text{ mg/mL}$) at different T (see legend). The plot shows the quantity $g_1(\tau) = \langle I_s(t)I_s(t+\tau) \rangle / \langle I_s(t) \rangle^2$, with I_s being the scattered intensity. (I) Sketch of the structural element possibly at the basis of ISO2 ordering: terminal Gs of eight distinct GCCG molecules assemble in two stacked G-quadruplexes. At large enough GCCG concentration, this structure is expected to be more stable than the Watson–Crick duplexing.

The presence of isotropic fluid on both sides of the diagram makes this phase diagram analogous to those reported for surfactant solutions where often lamellar and hexagonal phases are limited in both larger and smaller concentrations by isotropic micellar solutions.²⁰ This topology of the phase diagram in which the ordered phase is surrounded by isotropic fluid is also found for binary mixtures in which mixing is more favored in the ordered phase than in the disordered one such as found in mixtures of enantiomers in which the liquidus curve

has a maximum.²¹ The point of maximum stability, *i.e.*, the vertex of the bell-shaped envelope of the ordered phase (COLX in our case), is a first-order transition in which the transformation is discontinuous in T (with no phase coexistence) as in a single component system.

In our case, however, the diagram shows some degree of nonideality since the COLX and the COLX–ISO coexistence do not merge at a single point: in the T interval 45–50 °C the COLX phase can be found only in coexistence with the ISO

phase, while 45 °C is the largest T at which a homogeneous COLX phase can be found. This is clearly incompatible with a two-component system, but it is easily understood as an effect of minor residual impurities, which are revealed by osmolarity measurements as discussed in the SI. This nonideality is also revealed by measuring the concentration of coexisting ISO and LC phases. This measurement was performed by preparing three narrow capillaries, which were allowed to equilibrate and then centrifuged: a $c_{\text{DNA}} = 350 \text{ mg/mL}$ GCCG capillary centrifuged at $T = 22 \text{ }^{\circ}\text{C}$, a $c_{\text{DNA}} = 600 \text{ mg/mL}$ GCCG at $T = 32 \text{ }^{\circ}\text{C}$, and a $c_{\text{DNA}} = 600 \text{ mg/mL}$ ATTA at $T = 22 \text{ }^{\circ}\text{C}$. These capillaries were cut at the meniscus, and the concentrations were measured by UV absorption. Results are shown in parts A and B of Figure 2 as larger dots over a gray shading. In all cases, the difference in c_{DNA} between the two phases is on the order of 50 mg/mL, in line with our previous observations^{7,8} and theory.¹⁸ This value is markedly smaller than the width of the coexistence regions in parts A and B of Figure 2, again revealing the presence of an additional component which partitions between the two phases, effectively widening their coexistence.

Characteristics of the Phases of GCCG. *Chiral Nematic (N^*) Phase.* The GCCG N^* phase is characterized by a left-handed helical precession of the director and by helical pitches in the range 1–5 μm and growing with T and with c_{DNA} . Handedness and value of the N^* pitch are known to be the outcome of a subtle balance of competing forces.²² The handedness as well as the T and c_{DNA} dependence of the GCCG N^* phase are the same as those observed in the N^* phase of DNA duplexes when the nematic ordering develops at low enough DNA concentration, typically when $c_{\text{DNA}}(\text{ISO}-N^*) < 650 \text{ mg/mL}$ ²³ as in this specific case. Under these conditions, the side-to-side distance between parallel helices is large enough so that the N^* chirality is dominated by the electrostatic interactions between the phosphate chains favoring left-handed phase chirality.^{22–24} Further data and discussion are available in the SI.

Columnar Crystal (COLX) Phase. Figure 3A shows polarized transmission light microscope pictures of the COLX phase in coexistence with the ISO phase. The hallmark of the columnar phase in DNA solutions, first identified by Livolant and co-workers, are the conformal domains in which the local columnar axes lie on set of nested circles, a structure indicating repulsive interactions between adjacent columns that allow for their free sliding along the column axis.²⁵ This is the columnar texture also typically found in LCs of oligomeric DNA and RNA as well as in ATTA (Figure 1D). By contrast, the columnar texture found in GCCG indicates that the optical axis is uniform in each domain, as confirmed by the simultaneous extinction of the transmitted light from the whole domain (Figure 3B). Indeed, despite the many observations of this phase in GCCG samples, we have never observed the typical fan-shaped textures. This indicates that bend-type distortions of the director, allowed by the symmetry of the columnar phase, the flexibility of the columns, and their ability to slide past one another, are in GCCG instead suppressed.

We measured the birefringence Δn of the COLX GCCG domains and found $\Delta n/c_{\text{DNA}} \approx 6.2 \pm 0.4 \times 10^{-5} \text{ l/g}$, consistent with the birefringence of the columnar phase measured in solutions of DNA oligomers²³ and polymers.^{26,27} This indicates that paired bases in the COLX phase are ordered with their normal along the optical axis as in the conventional DNA columnar phase. Since any other arrangement would decrease the degree of orientational order of the bases and thus

significantly lower the birefringence, we understand the COLX phase as a columnar phase with additional side correlation among the columns forbidding bend deformation. In other words, we understand the COLX phase as a crystal-columnar phase.

Given the symmetry of the system, side–side interactions between columnar aggregates of GCCG and ATTA must reflect its two-base-long structural periodicity, as sketched in Figure 3C. Such periodicity might cause a two-base-long modulation of shape, and/or flexibility, and/or charge distribution. A possible source of these are transient unbindings of terminal pairs at each coaxial stacking position. Quite clearly, any of these modulations might induce longitudinal locking between neighboring columns, their loss of sliding freedom driving the COL phase to crystallize. An analogous longitudinal locking has been predicted for LC phases of screwlike particles with sufficiently pronounced helical shape.²⁸

A simple demonstration that column periodicity promotes stability of the GCCG COLX phase is offered by observing the effect of adding EtBr to the DNA solutions ($[\text{EtBr}] \approx [\text{GCCG}]/2$). Since EtBr randomly intercalates between paired bases, it acts as a local stretcher of the helical structure, thus disrupting its periodicity, as sketched in Figure 3D. Observations of LC textures by polarized light microscopy systematically confirm that the insertion of EtBr in the system eliminates the crystal character of COLX, transforming it into a standard bend-prone columnar LC phase, as shown in Figure 3E,F. The optical axis of the GCCG–EtBr phase (blue light line in Figure 3E), corresponding to the direction of low refractive index (i.e., along the duplex axis), is free to bend, enabling the typical columnar fan-shaped LC textures.

The formation of COLX in GCCG can be understood as the result of two effects. First, the onset of slide-forbidding correlations is made simpler in ultrashort oligomers. A simple estimate of the entropic penalty involved in the longitudinal locking of the columns is given by $\Delta S_L \approx k_B \ln(\delta/\Lambda)$, where $\Lambda \approx 6.6 \text{ \AA}$ is the period along the GCCG aggregate and δ is the sliding freedom of locked columns, likely of the range of one interbase distance $\delta \approx 3 \text{ \AA}$. This estimate suggests that the locking of GCCG occurs for interaggregate longitudinal interaction of the order of $\Delta G_L \approx 1k_B T$. In the case of longer LC-forming oligomers Λ becomes larger, and with it the entropic penalty to longitudinally lock the columns. Second, we find the locking mechanism to be present in GCCG but not in ATTA. This could be a consequence of larger shape modulations of GCCG. A further possibility to account for this difference is the richer arrays of modes of interaction available for guanosines (G), which are known to be able to form H-bonds between molecular positions not involved in conventional Watson–Crick pairing, such as those between Gs in the so-called G-quadruplexes⁴ (shown in Figure 3G). It is thus possible that as G terminals transiently unbind from the duplex aggregate they bond with G's, which are part of neighboring columnar aggregates, contributing to the longitudinal locking of the columns.

Dense Isotropic Phase. One of the most intriguing features of the GCCG phase diagram is the LC phases being delimited by the ISO phase on both the low density and the high-density sides. While we certainly expect the presence of an ISO phase at low c_{DNA} and high T where the degree of GCCG association is lower, the presence of a large c_{DNA} , low T ISO2 phase is specific for GCCG, since all other oligos we have considered in our

previous studies develop, in that limit, some form of birfringent crystalline structure.

The ISO2 phase appears to change continuously and directly into the ISO phase while remaining optically isotropic, which makes this transition difficult to observe optically in cells and capillaries at large c_{DNA} . However, even after careful inspection of flat cells prepared at $c_{\text{DNA}} = 700 \text{ mg/mL}$, at no T could we observe meniscuses separating distinct isotropic regions. Indeed, in the case of a first-order transition, as expected if ISO2 were an isotropic crystalline state, we would expect to see interfaces made detectable by the concentration difference between the phases. In such cells, what instead can be clearly observed is a marked change in viscosity as T rises above 40 °C (see the SI). Moreover, preliminary X-ray diffraction confirms the absence of crystalline peaks (see the SI).

To gain a better sense of the effect of cooling on samples at large c_{DNA} , we performed dynamic light scattering (DLS) on the sample contained in capillary 4 of Figure 2C after having dissolved in it a small amount of colloidal particles 100 nm diameter. Due to the small size of the capillary, we could not perform a reliable study as a function of the scattering vector. However, we could measure the intensity correlation functions $g_2(\tau) = \langle I_S(t)I_S(t + \tau) \rangle_t / \langle I_S(t) \rangle_t^2$ at fixed geometry (scattering angle ~90°) at various T . Figure 3H shows the squared field correlation function $lg_1(\tau)^2 = (g_2(\tau) - g_2(\infty)) / (g_2(0) - g_2(\infty))$ for three different T . At large T ($T = 65 \text{ }^\circ\text{C}$), where at visual inspection the solution appears fluid (see SI), we observe a single polydisperse decay indicating some degree of colloidal aggregation. The characteristic time of the fastest components of the decay suggests that the viscosity of the solution, even at this large T where we do not expect any structure, is up 10 times larger than pure water. This is expected, given the large c_{DNA} . As T decreases at and below values at which the solution appears to be a gel (see SI), a second feature appears in the correlation at shorter times, whose amplitude grows upon while its characteristic time slows down. This feature must be a manifestation of growing GCCG concentration fluctuation related to the increased intermolecular interactions, although no clean description of this is available at this stage. In the same range the main, slower feature markedly slows down, reaching the upper limit of measurable correlation times. In the interval 65–35 °C, the relaxation due to colloidal diffusion slows down more than 3 orders of magnitude, indicating an analogous growth of the viscosity. For even lower T , the scattered light shows the typical features of nonergodic systems, such as a low contrast of the time-averaged correlation functions.

This simple observation of the dynamics of scattered light indicates that the transition to ISO2 is associated with a strong increase of viscosity and kinetic attest, a behavior that closely resembles the continuous gelation observed in DNA hydrogels.²⁹ While determining molecular structure of ISO2 will require further structural analysis such as X-ray diffractometry, it is worth noticing that it is indeed expected that the liquid crystal ordering of a molecule such as GCCG would become unstable at large enough concentration. Because of the large fraction of G in the sequence, as c_{DNA} increases structure based on G-quadruplexes (Figure 3G) become more stable than those based on Watson–Crick pairing. This is because the equilibrium concentration of G-quadruplexes depends on $[G]^4$, the fourth power of the concentration of Gs,³⁰ while Watson–Crick pairs depend on c_{DNA}^2 . Moreover, G-quadruplets can stack on each other and the equilibrium concentration of two stacked G-quadruplexes depends on

$[G]^8$. Consider, for example, an aggregation motif involving G-octuplets as the one sketched in Figure 3I, consisting of pairs of stacked G-quadruplexes formed by the terminal Gs of eight distinct GCCG molecules. This structure is expected to become energetically favorable over Watson–Crick running-bond linear aggregates at rt for concentrations larger $[G] \approx 1 \text{ M}$ ($c_{\text{DNA}} \approx 650 \text{ mg/mL}$), which is where we indeed found the COLX-ISO2 transition. In this evaluation, we adopted the thermodynamic parameters for G-quadruplexes given in ref 30 at rt (further discussion in SI). Moreover, a simple estimate of the volume occupied by the repeating unit in Figure 3I is of the order of 10 nm³, matching $8 \text{ L}/N_A \approx 12 \text{ nm}^3$ (where L indicates liters), the volume available to each unit calculated on the basis of the GCCG concentration at $[G] \approx 1 \text{ M}$.

CONCLUSIONS

In this study, we investigated and quantitatively analyzed the phase behavior of the DNA oligomers ATTA and GCCG, whose sequence favors a running-bond staggered linear aggregation. Despite their expected weak bonding, these four-base-long oligomers are here reported to feature a rich phase diagram including N* and COL liquid crystal phases analogous to those previously reported for longer DNA oligomers and COLX and ISO2 molecular ordering, not observed previously in DNA solutions.

By adopting a recently developed model for the end-to-end assembly and liquid crystal ordering of cylindrical particles, we find a very good agreement between the thermal stability of the linear aggregates measured at various DNA concentrations and the phase boundary marking the appearance of liquid crystal ordering. Our analysis also leads to an alternative determination of the strength of the contribution of coaxial stacking to the duplex stability. Indeed, because of their heavily segmented structure, the aggregate of GCCG and ATTA appear to be ideal systems to provide a more solid deduction of the thermodynamic parameters for coaxial stacking, so far known only rather loosely.

The columnar crystal COLX and the dense isotropic ISO2 phases are found in GCCG solutions and are here interpreted as a possible effect of the interactions between guanosines. Indeed, the H-bonding between G's could indeed provide additional interactions between distinct GCCG double-helical aggregates, thus suppressing their freedom to slide along the columnar axis. Moreover, the thermodynamic stability of G-quartets and octets determined in previous studies supports the notion that at large enough concentration the system should prefer aggregation states alternative to the linear aggregates, as experimentally found.

Overall, the discovery of LC phases in DNA 4mers complements previous observations of LC phases in solutions of random-sequence oligomers⁸ and in multicomponent mixtures,⁷ confirming the remarkable capacity of nucleic acids to develop long-range fluid ordering. We previously speculated that these modes of self-assembly could have played a role in the prebiotic appearance of nucleic acids.¹² The results described here strengthen this notion and open to the possibility of the existence of ordered phases in solutions of even shorter oligomers.

METHODS

Synthesis and Purification. DNA 4-mers were assembled on an Äktalab Oligopilot synthesizer (Amersham Biosciences; GE Healthcare, Freiburg, D) in a 1.2 mL fixed volume column using standard

DNA phosphoramidites. Syntheses were started on dT base-loaded CPG, pore size 600 Å, loaded to 70 μmol/g (Prime Synthesis, Aston, PA). The introduction of the 3'-phosphate modification was achieved by coupling chemical phosphorylation reagent (Link Technologies, Bellshill, UK). A capping–oxidation–capping cycle was applied. Cleavage and deprotection were achieved by 90 min treatment with 40% aq MeNH₂ solution. This treatment not only cleaves the oligonucleotide from the solid support and removes all protective groups but also releases the 3'dT, thus yielding 3'-phosphate-modified 4-mer.³¹ After cleavage and deprotection, the product was harvested by filtration and 50% EtOH wash. The filtrate was evaporated to dryness and then reconstituted in 1 mL water. To this solution was added 100 μL of a 3 M NaAc solution, and the oligonucleotide was precipitated by addition of 14 mL of MeOH/BuOH (1/3, v/v) to remove acrylonitrile and acylamides from cleavage and deprotection. The precipitate was collected by centrifugation and decantation and washed with acetone. This precipitation procedure was repeated. The final pellet was dissolved in 5 mL of water and further purified by size-exclusion chromatography (Sephadex G25, GE Healthcare Europe, Freiburg, Germany) to remove excess salt and 5'-phosphate-dT. This process yielded 796 OD (26.3 mg, 20.9 μmol) of 5'-GCCGp-3' and 888 OD (29.3 mg, 23.4 μmol) of 5'-ATTAp-3'. Purity and identity were confirmed by IEX- and RP-HPLC and LC–MS (ESI-).

Sample Preparation. Stock solutions of ATTA and GCCG were prepared in Milli-Q water at $c_{DNA} = 100 \text{ mg/mL}$ (~85 mM) and stored at 4 °C. No salt was added, and the ionic strength was provided by the dissociation of the phosphate groups only. Three classes of samples were studied.

(1) Thin flat cells were prepared by progressively depositing 0.5–1 μL droplets of the stock solutions on flat glass (3 × 1.25 × 0.09 cm) and letting them dry until the required concentration is achieved. The cells were then closed, sealed with a fluorinate oil, and glued. The cell gap was provided by 20 μm silica spacers. Cell thickness and c_{DNA} were measured by performing microscope-based interferometry in different spots of the cell, *i.e.*, across the fluorinated oil and across DNA solutions in isotropic phase (at large T).

(2) A Vitrocom round capillary of 1.5 mm inner diameter was prepared by inserting 5.6 mg of lyophilized GCCGp in the bottom of the tube and serially adding water, spanning a total volume in the range 6–20 μL.

(3) Thinner capillaries, 0.6 mm inner diameter, were prepared by sucking 2–4 μL of DNA solution at the desired concentration and flame-sealing. After DNA sedimentation upon centrifugation at 3.5 × 10³ g in a T -controlled Eppendorf 5702RH centrifuge, the capillaries were cut at the meniscus between phases. The content of the resulting capillaries sections was diluted in 50 μL water and measured by 260 nm absorption with Evolution 300 UV–vis spectrophotometer (Thermo Scientific). Separation of coexisting phases from centrifuged thin capillaries were used to measure in each phase DNA concentration—via UV absorbance—and the osmolarity—via freeze point depression.

Optical Microscopy, Osmolarity Measurements, and Light-Scattering Measurements. Phase observations and fluorescence measurements were obtained with polarized optical microscopes TE300 and Abbe Optiphot 2 (Nikon) equipped with a Nikon DS-U1 color camera and Jenoptik b/w fluorescence camera. The temperature was controlled by Instec TSA02i hot and cold stages.

Dynamic light-scattering measurements were performed on a ST100 SciTech Instruments apparatus, customized to measure samples with small volume. Measurements were performed with a 532 nm solid-state laser source at 60° scattering angle.

Osmolarity was measured with a Gonotec Osmomat 030 (Gonotec, Berlin, Germany) freezing point osmometer. To perform the measurements, samples were adjusted to 5 mM concentration in water, and a 50 μL aliquot was used for the measurement.

ASSOCIATED CONTENT

S Supporting Information

The Supporting Information is available free of charge on the ACS Publications website at DOI: 10.1021/acsnano.6b03622.

Additional information on the aggregation model, aggregate thermal stability, coaxial-stacking energy values, prediction of the isotropic-LC transition, osmolarity measurements, G-quartets vs duplex equilibrium, and further data on phase characterization (PDF)

AUTHOR INFORMATION

Corresponding Author

*E-mail: tommaso.bellini@unimi.it.

Author Contributions

T.B., N.A.C., G.Z., T.P.F., and G.P.S. conceived the experiment; T.P.F. measured phase diagrams and thermal stability; T.B. adapted the aggregation model to analyze the data; G.N. performed the DLS measurements; L.B. and S.K. synthesized the oligomers and performed osmolarity measurements; T.B., N.A.C., G.Z., and T.P.F. wrote the manuscript.

Notes

The authors declare no competing financial interest.

ACKNOWLEDGMENTS

We acknowledge Carsten Tschierske, Paolo Mariani, David M. Walba, and Marco Todisco for useful suggestions and stimulating discussions. This work was supported by the PRIN Grant Program of the Italian MIUR Ministry, NSF MRSEC Grant Nos. 0820579 and 1420736, and NSF Biomolecular Materials Grant No. 1207606.

REFERENCES

- (1) Jones, M. R.; Seeman, N. C.; Mirkin, C. A. Programmable Materials and the Nature of the DNA Bond. *Science (Washington, DC, U. S.)* **2015**, *347*, 1260901–1260901.
- (2) Biffi, S.; Cerbino, R.; Bomboi, F.; Paraboschi, E. M.; Asselta, R.; Sciortino, F.; Bellini, T. Phase Behavior and Critical Activated Dynamics of Limited-Valence DNA Nanostars. *Proc. Natl. Acad. Sci. U. S. A.* **2013**, *110*, 15633–15637.
- (3) Um, S. H.; Lee, J. B.; Park, N.; Kwon, S. Y.; Umbach, C. C.; Luo, D. Enzyme-Catalysed Assembly of DNA Hydrogel. *Nat. Mater.* **2006**, *5*, 797–801.
- (4) Davis, J. T.; Spada, G. P. Supramolecular Architectures Generated by Self-Assembly of Guanosine Derivatives. *Chem. Soc. Rev.* **2007**, *36*, 296–313.
- (5) Cafferty, B. J.; Gallego, I.; Chen, M. C.; Farley, K. I.; Eritja, R.; Hud, N. V. Efficient Self-Assembly in Water of Long Noncovalent Polymers by Nucleobase Analogues. *J. Am. Chem. Soc.* **2013**, *135*, 2447–2450.
- (6) Nakata, M.; Zanchetta, G.; Chapman, B. D.; Jones, C. D.; Cross, J. O.; Pindak, R.; Bellini, T.; Clark, N. A. End-to-End Stacking and Liquid Crystal Condensation of 6 to 20 Base Pair DNA Duplexes. *Science* **2007**, *318*, 1276–1279.
- (7) Zanchetta, G.; Nakata, M.; Buscaglia, M.; Bellini, T.; Clark, N. A. Phase Separation and Liquid Crystallization of Complementary Sequences in Mixtures of nanoDNA Oligomers. *Proc. Natl. Acad. Sci. U. S. A.* **2008**, *105*, 1111–1117.
- (8) Bellini, T.; Zanchetta, G.; Fraccia, T. P.; Cerbino, R.; Tsai, E.; Smith, G. P.; Moran, M. J.; Walba, D. M.; Clark, N. A. Liquid Crystal Self-Assembly of Random-Sequence DNA Oligomers. *Proc. Natl. Acad. Sci. U. S. A.* **2012**, *109*, 1110–1115.
- (9) Zanchetta, G.; Bellini, T.; Nakata, M.; Clark, N. A. Physical Polymerization and Liquid Crystallization of RNA Oligomers. *J. Am. Chem. Soc.* **2008**, *130*, 12864–12865.

- (10) Selinger, J. V.; Bruinsma, R. F. Hexagonal and Nematic Phases of Chains. I. Correlation Functions. *Phys. Rev. A: At., Mol., Opt. Phys.* **1991**, *43*, 2910–2921.
- (11) Gilbert, W. The RNA World. *Nature* **1986**, *319*, 618.
- (12) Fraccia, T. P.; Smith, G. P.; Zanchetta, G.; Paraboschi, E.; Yi, Y.; Walba, D. M.; Dieci, G.; Clark, N. A.; Bellini, T. Abiotic Ligation of DNA Oligomers Tempered by Their Liquid Crystal Ordering. *Nat. Commun.* **2015**, *6*, 6424.
- (13) Fraccia, T. P.; Zanchetta, G.; Rimoldi, V.; Clark, N. A.; Bellini, T. Evidence of Liquid Crystal–Assisted Abiotic Ligation of Nucleic Acids. *Origins Life Evol. Biospheres* **2015**, *45*, 51–68.
- (14) Cates, M. E.; Candau, S. J. Statics and Dynamics of Worm-like Surfactant Micelles. *J. Phys.: Condens. Matter* **1990**, *2*, 6869–6892.
- (15) SantaLucia, J.; Hicks, D. The Thermodynamics of DNA Structural Motifs. *Annu. Rev. Biophys. Biomol. Struct.* **2004**, *33*, 415–440.
- (16) Peyret, N. *Prediction of Nucleic Acid Hybridization: Parameters and Algorithms*; Wayne State University: Detroit, 2000.
- (17) Yakovchuk, P.; Protozanova, E.; Frank-Kamenetskii, M. D. Base-Stacking and Base-Pairing Contributions into Thermal Stability of the DNA Double Helix. *Nucleic Acids Res.* **2006**, *34*, 564–574.
- (18) Kuriabova, T.; Betterton, M. D.; Glaser, M. A. Linear Aggregation and Liquid-Crystalline Order: Comparison of Monte Carlo Simulation and Analytic Theory. *J. Mater. Chem.* **2010**, *20*, 10366–10383.
- (19) De Michele, C.; Bellini, T.; Sciortino, F. Self-Assembly of Bifunctional Patchy Particles with Anisotropic Shape into Polymers Chains: Theory, Simulations, and Experiments. *Macromolecules* **2012**, *45*, 1090–1106.
- (20) Mitchell, J.; Tiddy, G. J. T.; Waring, L.; Bostock, T.; McDonald, M. P. Phase Behaviour of Polyoxyethylene Surfactants with Water. *J. Chem. Soc., Faraday Trans. 1* **1983**, *79*, 975–1000.
- (21) Rastogi, R. P. Thermodynamics of Phase Equilibria and Phase Diagrams. *J. Chem. Educ.* **1964**, *41*, 443.
- (22) Kolli, H. B.; Frezza, E.; Cinacchi, G.; Ferrarini, A.; Giacometti, A.; Hudson, T. S.; De Michele, C.; Sciortino, F. Self-Assembly of Hard Helices: A Rich and Unconventional Polymorphism. *Soft Matter* **2014**, *10*, 8171–8187.
- (23) Zanchetta, G.; Giavazzi, F.; Nakata, M.; Buscaglia, M.; Cerbino, R.; Clark, N. A.; Bellini, T. Right-Handed Double-Helix Ultrashort DNA Yields Chiral Nematic Phases with Both Right- and Left-Handed Director Twist. *Proc. Natl. Acad. Sci. U. S. A.* **2010**, *107*, 17497–17502.
- (24) Rossi, M.; Zanchetta, G.; Klussmann, S.; Clark, N. A.; Bellini, T. Propagation of Chirality in Mixtures of Natural and Enantiomeric Dna Oligomers. *Phys. Rev. Lett.* **2013**, *110*, 107801.
- (25) Livolant, F.; Levelut, A. M.; Doucet, J.; Benoit, J. P. The Highly Concentrated Liquid-Crystalline Phase of DNA is Columnar Hexagonal. *Nature* **1989**, *339*, 724–726.
- (26) Brandes, R.; Kearns, D. R. Magnetic Ordering of DNA Liquid Crystals. *Biochemistry* **1986**, *25*, 5890–5895.
- (27) Oldenbourg, R.; Ruiz, T. Birefringence of Macromolecules. Wiener's Theory Revisited, with Applications to DNA and Tobacco Mosaic Virus. *Biophys. J.* **1989**, *56*, 195–205.
- (28) Kolli, H. B.; Frezza, E.; Cinacchi, G.; Ferrarini, A.; Giacometti, A.; Hudson, T. S. Communication: From Rods to Helices: Evidence of a Screw-like Nematic Phase. *J. Chem. Phys.* **2014**, *140*, 081101.
- (29) Biffi, S.; Cerbino, R.; Nava, G.; Bomboi, F.; Sciortino, F.; Bellini, T. Equilibrium Gels of Low-Valence DNA Nanostars: A Colloidal Model for Strong Glass Formers. *Soft Matter* **2015**, *11*, 3132–3138.
- (30) Mariani, P.; Spinozzi, F.; Federiconi, F.; Amenitsch, H.; Spindler, L.; Drevensek-olenik, I. Small Angle X-Ray Scattering Analysis of Deoxyguanosine 5'-Monophosphate Self-Assembling in Solution: Nucleation and Growth of G-Quadruplexes. *J. Phys. Chem. B* **2009**, *113*, 7934–7944.
- (31) Horn, T.; Urdea, M. S. A Chemical 5'-Phosphorylation of Oligodeoxyribonucleotides That Can Be Monitored by Trityl Cation Release. *Tetrahedron Lett.* **1986**, *27*, 4705–4708.